Dynamic Models for Shimmy Analysis of Helicopter Landing Gear *

M. Grossini[1], E. Carrera[1] and A. Abbá[2]
(1) Aerospace Department, Politecnico di Torino, Torino, Italy.
(2) Mecaer, Borgomanero, Italy.

abstract

The present work deals with dynamic models for the analysis of shimmy phenomenon of helicopter A109 landing gear. The investigation has been conducted accounting for different models. In the first ones, shimmy has been faced with analitical simplified approaches. The equations of motion has been written according to two multibody models with two and five degrees of freedom respectively. Linear and non linear cases have been solved. A parametric analysis shows the influence of some geometrical and mechanical properties, like the caster lenght and the stem stiffness. The same problem has been implemented then by using the multibody dynamics code ADAMS: in this case, the analysis was principally based on the joints and on the contact conditions represented by the dynamic and static friction parameters.

*The content of this paper has been partially presented at EUROMECH-427, Cachan, Paris, 24-27 Sept. 2001.

1 Introduction

The landing gear dynamic plays an important role in the aircraft design. Take off and landing represent in fact severe load conditions. Landing gear system has to resist to the landing and to damp as soon as possible the aircraft kinetic energy avoiding too much high dangerous deceleration. During the landing, the landing gear system has to assure a stable rolling on the runway, avoiding dangerous lateral skids that can lead the aircraft out of the runway. A violent vibration of the nose landing gear about the spindle axis, i.e. shimmy phenomenon, can appear in such case. Although these vibrations are not usually catastrophic, they can lead to accidents due to excessive wear and shortened life of gear parts and contribute to pilot and passenger discomfort.

The shimmy phenomenon is very much related to the mechanical behaviour of tire. Many mathematical models were developed to obtain forces and moments on the tire: "the elastic string theory" of Dietrich, V. Schlippe, Pacejka and " the point of contact method" of Moreland [1],[2],[4],[5]. It seems that these models give suitable results, but these are difficult to be compared. In the present work, "the string elastic theory" is employed.

The dynamic models presented are related to the three-wheeler landing gear helicopter A109. Although it can be unusual to treat the shimmy phenomenon of helicopters, it should be underlined that the landing and take-off taxing is a common procedure for helicopter equiped with landing gears. Of course, the helicopter taxing speeds are lower than the airplane taxing speeds: but not so low to grant a safe taxing. The A109 specifications, in fact, say that "a safe taxing has to be granted till 20 [knots]". This means that taxing instability problems can appear.

2 Preliminary

2.1 Tire mathematical model

Many mathematical models describing the tire mechanical behaviour can be found in technical literature [1],[2],[4]. In the present work, a semiempirical model, derived in part from experimental tests and in part from semiempirical formulas [3], is adopted. In fact, vertical reaction force vs. tire vertical deflection and lateral spring constant have been evaluated from experimental tests. The others characteristic have been derived by using the semiempirical formulas showed in Appendix A. In figure 4 the vertical reaction force vs. tire deflection has been represented. In figure 5 the lateral spring constant vs. vartical reaction force has been represented. In figure 3 tire footprint has been represented.

2.2 Vertical reactions on landing gears

The vertical reactions on landing gears can be derived from forces and momentums equilibrium equations. Neither rolling nor pitching rotations are considered: so the vertical reactions are constant and are expressed by the following relations:

$$N_1 + 2N_2 = mg \tag{1}$$

$$N_1 l_1 = 2N_2 l_2 \tag{2}$$

Therefore:

$$N_1 = \frac{l_2}{l_1 + l_2} mg \tag{3}$$

$$N_2 = \frac{1}{2} \frac{l_1}{l_1 + l_2} mg \tag{4}$$

Through the vertical reactions, it is possible to calculate all the tire mechanical properties such as elastic spring constant and relaxation length (figure 4-5 and Eq. 17-28).

2.3 Friction in the bearings

The friction in the bearings of the oil pneumatic shock absorber, can be evaluated considering the reaction forces on the bearings (see figure 1). The reaction forces R_1 and R_2 can be calculated from these two equilibrium equation:

$$\begin{cases} R_1 (x + c) - Nz - R_x (b - x) = 0 \\ R_2 (x + c) - Nz - R_x (b + c) = 0 \end{cases} \tag{5}$$

where $R_x = \mu_{volv} N$, $\mu_{volv} = 0.013 + 0.0000065 V^2$ (see [1]) and N is the vertical reaction force on the tire.

Therefore:

$$\begin{cases} R_1 = \frac{N(z + \mu_{volv}(b-x))}{x+c} \\ R_2 = \frac{N(z + \mu_{volv}(b+c))}{x+c} \end{cases} \tag{6}$$

The modulus of the friction torque can be evaluated with this relation:

$$|M_{bearing}| = \mu_{bearing} (r_{b1} R_1 + r_{b2} R_2) \tag{7}$$

where r_{b1} and r_{b2} are the the bearing radius.

Finally it follows that the friction torque is:

$$M_{bearing} = |M_{bearing}| \left(\dot{\vartheta}_1 - \dot{\vartheta}_2 \right) \tag{8}$$

2.4 Nose landing gear inertia momentum

The landing gear total inertia momentum around the spindle axes, is represented by the following contributes: J_s stem inertia moment, J_f fork inertia moment, J_p tire inertia moment, J_t transport inertia moment. Therefore:

$$J_c = J_s + J_f + \frac{J_p}{2} + J_t \tag{9}$$

Where:

$$J_f = k_f m_f z^2$$

The spin tire inertia moment can be calculated with an approximated approach, considering the tire and the hubcap as two cylinders, therefore:

$$J_p = m_{pn} r_{pn}^2 + m_{ce} r_{ce}^2$$

where r_{pn} represents the tire medium radius, r_{ce} is the peripheral hubcap radius (the hubcap mass is mainly distributed around the hubcap peripheral radius), m_{pn} is the tire mass and m_{ce} is the hubcap mass. The transport inertia moment is:

$$J_t = z^2 \left(m_{pn} + m_{ce}\right)$$

3 Linear analytical models.

In the present section some results developed in MATLAB enviroment are showed. Linear and non-linear solutions are given.

3.1 Two degrees of freedom model.

This mathematical model is a two degrees of freedom model that neglects the whole helicopter dynamic: the only nose landing gear dynamic is considered. The first degree of freedom is represented by the nose landing gear yaw rotation around the spindle axis; the second degree of freedom is represented by lateral distortion of tire equator at center of tire-ground contact area (see figure 1 and figure 3).

The torsional dynamics of the lower parts of the landing gear is described by a 2nd order differential equation for the angle ϑ about the spindle axis:

$$-J_c \ddot{\vartheta} - \beta_z \dot{\vartheta} - F_y(z+t) - \beta_{z,pn} \dot{\vartheta} - G = 0 \tag{10}$$

The lateral distortion of the tire is described by the model of an elastic string theory. This is the lateral no-skid condition [1]:

$$V sin\left(\vartheta\right) + \left(z - a\right) \dot{\vartheta} - \frac{\sigma}{\sigma + a} \left(\dot{y} + V \frac{y}{\sigma}\right) = 0 \tag{11}$$

[1] where $y = \alpha \left(\sigma + a\right)$

The system of equation represented by Eq.10-11 consist of a non-linear system. For a first understanding of the dynamics, the nonlinear model is linearized and eigenvalues are computed, applying MATLAB routines. After linearization and reduction to the first order, the linear system reads:

$$\begin{cases} p - \dot{\vartheta} = 0 \\ V\vartheta + (z-a)\, p - \frac{\sigma}{\sigma+a}\left(\dot{y} + V\frac{y}{\sigma}\right) = 0 \\ -J_c - \beta_{z,pn} p - \beta_z p - K_y\,(z+t)\, y - C_G J_p \omega \frac{\dot{y}}{r} = 0 \end{cases} \tag{12}$$

This system can be rewritten by using matrix notation:

$$[A]\,\dot{\bar{r}} + [B]\,\bar{r} = 0 \tag{13}$$

Posing $\bar{r} = \bar{c}e^{\lambda_i t}$, eigenvalues λ_i are derived from the following matrix:

$$[M]_{stab} = -\,[A]^{-1}\,[B] \tag{14}$$

3.1.1 Stability curves in parameter space

The stability system analisy was performed respect a reference configuration 1 and through some parameters such as the taxing speed, the caster length, the damping rotation constant and the torque torsional stiffness(taxing with locked commands). The real part of eigenvalues (on the left) and the characteristic frequencies (on the right) are showed vs. the variation of taxing speed and caster length in figure 6. It can be easily seen that large values of taxing speed cause more instability; large values of relaxation length instead cause more stability. Therefore it is possible to stabilize the system adopting large value of the caster length. Nevertheless this method is usually not adopted because the landing gear slot is narrow and large values of caster length mean a more complex kinematic mechanism, too high fork bending moments and an increased mass of the landing gear. The real part of eigenvalues (on the left) and the characteristic frequencies (on the right) are showed vs. the variation of taxing speed and damping torque constant In figure 7 . It can be easily seen that large values of taxing speed cause more instability and that large values of damping constant cause more stability. Usually, the damping torque is mainly due to viscous friction in the bearings of the oil-pneumatic shock absorber and from shimmy damper. There are two groups of shimmy dampers. To the the first ones belongs oleodynamic dampers that produces damping with the oil drawing from the chambers of the damper: it can produce very large damping and it is usually adopted by large airplanes. To the second group belong dry friction dampers. In this work a dry friction ring fitted in the torque link revolving bearing is considered : the relative rotation between the stem (sliding member) and the leg of the landing gear causes dry friction. This solution is quite cheap and simple but it can be adopted only for small airplanes or helicopters. The

real part of eigenvalues (on the left) and the characteristic frequencies (on the right) are showed vs. the variation of taxing speed and stem stiffness in figure 8 . It can be easily seen that large values of taxing speed cause more instability and that large values of stem stiffness cause more stability. This kind of configuration is typical of taxing with locked commands. Military aircraft usually land on the aircraft carrier with locked commands because of the narrow runaway. Of course, this method produces a safe taxing but it doesn't allow to change the direction of taxing.

3.2 Five degrees of freedom model.

This mathematical model considers the dynamic of the whole mechanical system. These are the degree of freedom(see figure 2): nose landing gear absolute yaw angle ϑ_1, helicopter absolute yaw angle ϑ_2, nose landing gear tire lateral distortion y_1, main landing gear tire lateral distortion y_2(the same for each tire), helicopter lateral shift η. The equation of motion which describes the dynamic of the whole mechanical system are represented by the momentum equilibrium of the nose landing gear around the spindle axis, by the momentum equilibrium of the helicopter about the yaw axis, by the force equilibrium along the direction perpendicular to the taxing direction (nose landing gear and helicopter) and by two no lateral skid (respectively for nose landing gear and main landing gear) equations derived by string elastic theory. A damping torque was introduced for main landing gear not depending on taxing speed but only on lateral distortion speed $\dot{y_2}$. The total set of differential equation is summarized below:

$$\begin{cases} \dot{\eta} - l_1\dot{\vartheta}_2 + (z-a)\,\dot{\vartheta}_1 + V\vartheta_1 - \frac{\sigma_1}{\sigma_1+a}\left(\dot{y}_1 + V\frac{y_1}{\sigma_1}\right) = 0 \\ (l_2-a_2)\,\dot{\vartheta}_2 + V\vartheta_2 + \dot{\eta} - \frac{\sigma_2}{\sigma_2+a}\left(\dot{y}_2 + V\frac{y_2}{\sigma_2}\right) = 0 \\ -J_e\ddot{\vartheta}_2 - 2K_{y,2}\,(l_2+t_2)\,y_2 - 2\beta_{y,2}\,(l_2+t_2)\,\dot{y}_2 - F_1 l_1 + \\ -K_z\,(\vartheta_2-\vartheta_1) - (\beta_z+\beta_{z,pn})\left(\dot{\vartheta}_2-\dot{\vartheta}_1\right) = 0 \\ -J_c\ddot{\vartheta}_1 - (\beta_z+\beta_{z,pn})\left(\dot{\vartheta}_1-\dot{\vartheta}_2\right) - K_z\,(\vartheta_1-\vartheta_2) + \\ -K_{y,2}\,(z+t_1)\,y_1 - C_G J_p\omega\frac{\dot{y}_1}{r} = 0 \\ -m\ddot{\eta} - 2K_{y,2}y_2 - 2\beta_{y,2}\dot{y}_2 + F_1 = 0 \\ -m_c\left(\ddot{\eta} - l_1\ddot{\vartheta}_2 + b_{G,c}\ddot{\vartheta}_1\right) - K_{y,2}y_1 + F_1 = 0 \end{cases} \tag{15}$$

The equation of motion are 6 instead of 5 because the lateral reaction force F_1 (between the nose landing gear and the helicopter) is unknown. Solving for F_1, it is possible to lower the number of equation to 5. The resultant differential equations system can be reduced to the first order and rewritten the same notation given at Eq. 13-14.

3.2.1 Stability curves.

The stability analysis was performed only varying the taxing speed V for estimating the influence of the whole mechanical system on the nose landing gear dynamic presented in §3.1. In figure 9 the real part of eigenvalues (on the left) and the characteristic frequencies (on the right) are showed at variation of taxing speed. It can be easily seen that there are small differences between some eigenvalues found with the two degrees of freedom and with the 5 degrees of freedom model. It could be concluded that neglecting the helicopter dynamic consists of a good hypothesis. The others eigenvalues have all negative real part for every value of taxing speed. The helicopter dynamic is therefore always stable. In the frequency graph two characteristic frequency are showed. By comparing the two mathematical model, it is found that the highest frequency is mainly due to nose landing gear dynamic and the lowest frequency is mainly due to helicopter dynamic. The damping constant that makes stable the mechanical system, is showed in figure 10. From these results descend that the most critical velocity (with the highest damping constant) is 10.5[m/s]. Almost the same value will be found in non linear analysis.

4 Non linear analytical model

The dynamics of the system can be directly solved by numerical simulation with respect to time; even for large amplitudes where linearization no longer holds. This analysis was performed for testing a very simple and cheap damper system based on dry friction. This system consists of a isogliss (or carbogliss) ring with big dry friction constant: the ring is fitted in the torque link revolving bearing. The friction torque is constant and depends on the locking torque: the sign of the torque depends on the sign of the angular velocity.

Usually the locking torque is not calculated but it is determined through experimental test: from highest value of the torque (almost with locked commands) to lower ones till no shimmy phenomenon happens in the prescribed range of taxing speed.

4.1 Two degrees of freedom model.

In this section, the only nose landing gear dynamic is considered. Therefore two degrees of freedom are needed to describe the mechanical behaviour of the mechanical system. This model is completely non linear and it is referred to system of equation represented by Eq. 10-11. In this case an additional term due to dry friction torque is introduced in the rotation equilibrium equation.

$$C = (|M_{isogliss}| + |M_{bearing}|)\, sign\left(\dot{\vartheta}\right) \tag{16}$$

The locking torque can be considered proportional to the friction torque $M_{isogliss}$: the proportionality constant depends on the kind of bush adopted to lock the friction ring. In this work this constant was assumed to be 3.84.

4.1.1 Stability curves.

The numerical simulation has demonstrated that instability occurs for every taxing speed if the lateral perturbative load is below a critical stability value: this critical value depends on the taxing speed and the friction torque. The perturbative loading-time is assumed to be 0.01[s]: almost impulsive.

In figure 11 some results are showed. It can be easily seen that the highest critical speed that needs the largest damping is almost 11[m/s]: the same value was found in the linear analysis. The system is always stable for any given taxing speed value lower than 5[m/s]. For example, if the taxing has to be stable if the lateral load is below 200[N], a friction torque equal to 1[Nm] has to be adopted: this corresponds to have a locking torque equal to 0.384[daNm] (typical unit adopted by dynamometric wrench)

5 Description and results rolled by using ADAMS

A large investigation has been conducted by means of a general pourpose multibody code. The most representative results are showed in the present section.

The multibody code adopted is ADAMS, that is *Automatic Analysis of Mechanical Systems*. This code was chosen because its simplicity, reliability and robustness as well as its friendly to use interface.

5.1 ADAMS model

The present model include the whole helicopter but it neglects the vertical stiffness of the tire: only the lateral stiffness is considered.

The implemented ADAMS model includes: helicopter cell-case-main landing gear stems (one body), hubcap-axle groups (3 bodies), tires (3 bodies), stem-nose landing gear fork group (one body). The number of bodies is therefore equal to 8: this means 48 degrees of freedom.

The nose landing gear stem is joined to the fuselage with a revolute. The main landing gear hubcaps are joined to axles with revolutes. The nose landing gear hubcap is joined to stem-fork group with a revolute. The tires are joined to the hubcaps with a prismatic joint. The helicopter center of gravity has to stay in a plain.

Spring between the tires and hubcaps pretend the lateral spring constant of tires The contact between tires and runaway is circular and is described by these static and dynamic friction parameters: $\mu_{static} = 0.9$, $\mu_{dynamic} = 0.83$.

The helicopter taxing speed in x direction is fixed by a motion generator and it is equal to 11000[m/s]. The lateral perturbative load on the tire is equal to 250[N] for .01[s]: the force is applied after 0.19[s] from the beginning of the simulation.

In figure 12 two views of the helicopter are showed: the ellipsoid pretends all the inertial properties of the helicopter.

5.2 Results

The angular velocity and its FFT-module are showed vs. the variation of time in figure 13 . From the observation of FFT-module, it is possible to emphasize two main frequencies which correspond to the values 1.9[Hz] and 24[Hz]. These results confirm the previous analyses performed with MATLAB.

Moreover,observing the time-response, it is possible to recognize that the mechanical system is unstable because is underdamped.

In figure 14 the helicopter lateral shift is showed: the system is unstable.

Main landing gear tire lateral distortion has been plotted in figure 15. It is possible to notice that the two distortions are equal in module (the opposite sign is due to different reference system). It follows that to consider the main landing gear lateral distortions equal in the five degrees of freedom model, it is a right hypothesis.

Conclusions

Different models of helicopter shimmy has been analyzed in the present work. These all have led to comparable results. The ADAMS mechanical model has validate the hypothesis that were adopted to write the motion equations of simplified models.

Many other investigations can be performed about the lateral perturbative load that that induce the shimmy phenomenon: probably, these lateral perturbative loads are due to the runway caracteristic and to the aircraft weight. Experimental tests, about many kinds of aircraft, could provide important correlations between the principal parameters that describe the whole system.

These analyses could be important to find a right criteria about anti-shimmy design and to improve aircraft normative laws.

References

[1] Genta G. - Meccanica dell'autoveicolo. pp. 71-116.

[2] Pacejka H. B. - MF-Tyre User Manual Version 5.0 - Delft University of Technology.

[3] Smiley R. F., Horne W.B. - Mechanical Properties of Pneumatic Tires with Special Reference to Modern Aircraft Tires. - NACA Technical Report Note 4110.

[4] Bakker E., Nyborg L., Pacejka H. B. - Tyre modelling for use in vehicle dynamics studies. - SAE paper no. 870421, Feb. 1987.

[5] Robert F. Smiley. - Correlation, Evaluation, and Extension of Linearized Theories for Tire Motion and Wheel Shimmy. - NACA Report 1299

[6] Gerhard Somieski. - Shimmy Analysis of a Simple Aircraft Nose Landing Gear Model Using Different Mathematical Methods. - *Aerospace Science and Technology*, 1997, no. 8,pp. 545-555.

[7] Van der Valk R., Pacejka H. B. - An analysis of a civil aircraft main gear shimmy failure, *Vehicle System Dynamics*, 1993, 22,pp. 97-121.

List of symbols

α	slip angle $[rad]$
a	tire half footprint length $[m]$
A_g	footprint area $[m^2]$
A_n	net footprint area $[m^2]$
b	footprint width $[m]$
$b_{G,c}$	distance between nose-landing-gear center of gravity and the spindle axis. $[m]$
b_{sa}	characteristic length shock absorber [m]
$\beta_{y,2}$	linear damping coefficient for tires main landing gear $[Ns/m]$
β_z	torque damping coefficient $[Nms/rad]$
$\beta_{z,pn}$	tire torque damping coefficient$[Nms/rad]$
C	friction torque Nm
C_α	cornering power $[N/rad]$
c_{sa}	characteristic length shock absorber [m]
d	tire diameter $[m]$
F_y	lateral force $[N]$
F_z	vertical force $[N]$
G	gyroscopic torque $[Nm]$
g	gravity acceleration $[m/s^2]$
k_β	torque friction parameter
k_f	fork shape constant
K_x	fore-and-aft sring constant $[N/m]$
K_y o $K_{y,1}$	nose landing gear tire lateral spring constant$[N/m]$
$K_{y,2}$	main landing gear tire lateral spring constant$[N/m]$
J_c	nose landing gear inertia moment $[Kgm^2]$
J_e	helicopter inertia moment about yaw axis $[Kgm^2]$
J_s	stem inertia moment $[Kgm^2]$
μ_y	lateral static friction coefficient
l_1	distance between helicopter center of gravity and nose landing gear spindle axis $[m]$
l_2	distance between helicopter center of gravity and main landing gear $[m]$
m	helicopter mass $[Kg]$
m_{ce}	hubcap mass $[Kg]$
m_f	fork mass$[Kg]$
m_{pn}	tyre mass $[Kg]$
m_s	stem massa $[Kg]$
M_z	damping torque $[Nm]$
N_z	autoaligning torque $[Nm]$
p	tyre inflation pressure $[Pa]$
p_0	tyre inflation pressure at zero vertical load $[Pa]$
p_r	tyre rated inflation pressure$[Pa]$

List of symbols

r	tyre radius $[m]$
r_{b1} and r_{b2}	bearing radius $[m]$
s	tyre vertical deflection $[m]$
σ o σ_1	nose landing gear rolling relaxation length $[m]$
σ_2	main landing gear rolling relaxation length $[m]$
t o t_1	nose landing gear pneumatic caster $[m]$
t_2	main landing gear pneumatic caster $[m]$
ϑ o ϑ_1	nose landing gear absolute rotation $[rad]$
ϑ_2	helicopter absolute rotation $[rad]$
V	speed $[m/s]$
V_x	longitudinal speed $[m/s]$
V_{sy}	lateral slip velocity $[m/s]$
y o y_1	nose landing gear tire lateral deflection$[m]$
y_2	main landing gear tire lateral deflection $[m]$
x	crushing of the shock absorber $[m]$
ω	tyre spin $[rad/s]$
w	maximum width of undeflected tire $[m]$
z	caster $[m]$

A Mechanical properties of the tire.

1. Tire footprint length;

$$\frac{a}{d} = .85\sqrt{\frac{s}{d} - \left(\frac{s}{d}\right)^2} \tag{17}$$

2. Tire footprint width:

$$\frac{b}{w} = 1.7\sqrt{\frac{s}{w} - 2.5\left(\frac{s}{w}\right)^4 + 1.5\left(\frac{s}{w}\right)^6} \tag{18}$$

3. Gross footprint area:

$$A_g = 2.25\,(s - .03w)\,\sqrt{wd} \tag{19}$$

4. Net footprint area:

$$A_n = aA_g \tag{20}$$

dove $a \cong .675$

5. pressure rise (semiempirical):

$$\Delta p = n\kappa p_0 \left(\frac{s}{w}\right)^2 \tag{21}$$

where $\kappa = 1.5\frac{w}{d}$ and $n = 1$ for isotherm process. Therefore:

$$p = p_0 + \Delta p$$

6. Vertical force active on tire from ground:

$$\frac{F_z}{(p + 0.08p_r)\,w\sqrt{wd}} = 2.4\left[\frac{s}{w} - C_z\left(1 - e^{-\frac{.6\frac{s}{w}}{C_z}}\right)\right] \tag{22}$$

where C_z depends on tire type:

$$C_z = \begin{cases} 0.02 \text{ Type I} \\ 0.03 \text{ Type III e VII} \end{cases}$$

.

7. Average gross footprint pressure:

$$p_n = \frac{F_z}{A_n} \tag{23}$$

8. Lateral spring constant:

$$K_y = \tau_y w \left(p + 0.24 p_r\right) \left[1 - .7 \frac{s}{w}\right] \tag{24}$$

where τ_y depends on tire type:

$$\tau_y = \begin{cases} 3 \text{ Tipo I} \\ 2 \text{ Tipo III e VII} \end{cases}$$

.

9. fore-and-aft spring constant:

$$K_x = .8d \left(p + 4p_r\right) \sqrt[3]{\frac{s}{w}} \tag{25}$$

10. Relaxation length:

$$\frac{\sigma}{\left(2.8 - 0.8\frac{p}{p_r}\right) w} = \begin{cases} 11\frac{s}{d} \ \left(\frac{s}{d} \leq .053\right) \\ 64\frac{s}{d} - 500\left(\frac{s}{d}\right)^2 - 1.4045 \ \left(.053 \leq \frac{s}{d} \leq .068\right) \\ .9075 - 4\frac{s}{d} \ \left(.068 \leq \frac{s}{d}\right) \end{cases} \tag{26}$$

11. drag coefficient of friction:

$$\mu_y = .93 - .0011 p_n \tag{27}$$

12. Cornering power constant:

$$C_\alpha = \left(a + \sigma\right) K_y \tag{28}$$

13. Cornering force:

$$\frac{F_y}{\mu_y F_z} = \begin{cases} \phi - \frac{4}{27}\phi^3 \ \left(0 \leq \phi \leq 1.5\right) \\ 1 \ \left(\phi \geq 1.5\right) \end{cases} \tag{29}$$

where $\phi = \frac{C_\alpha}{\mu_y F_z}\alpha$.

14. Moment parameter:

$$\frac{t}{a} = \begin{cases} \frac{.8}{1 - \frac{4}{27}\phi^2} \ \left(\phi \leq .1\right) \\ \frac{\left(\phi - \phi^2 - .01\right)}{\phi - \frac{4}{27}\phi^3} \ \left(.1 \leq \phi \leq .55\right) \\ \frac{.2925 - .1\phi}{\phi - \frac{4}{27}\phi^3} \ \left(.55 \leq \phi \leq 1.5\right) \\ .2925 - .1\phi \ \left(\phi \geq 1.5\right) \end{cases} \tag{30}$$

15. Self aligning torque:

$$N_z = tF_y \tag{31}$$

16. Lateral damping constant:

$$\beta_z = k_\beta \frac{a^2 C_\alpha}{V} \tag{32}$$

17. Damping torque:

$$M_z = \beta_z \dot{\vartheta} \tag{33}$$

where ϑ is the angular position of the nose landing gear.

18. Gyroscopic torque(in case of low distortions):

$$G = C_G J_p \omega \frac{\dot{y}}{r} \tag{34}$$

where C_g is a correction parameter and $\omega \cong \frac{V}{r}$. It was assumed that $C_G = .4$.

If there isn't tire lateral skidding (only if the lateral perturbative load is smaller than the friction lateral load), the string elastic hypothesis is correct and the lateral speed of the point of contact respect to the tire medium plane, must be equal to zero.

$$\dot{y_1} + \frac{V_x}{\sigma} y_1 - V_{sy} = 0 \tag{35}$$

where y_1 is the lateral distortion of the first point of contact, V_x is the taxing speed and V_{sy} is the lateral slip speed of the tire [2],[6],[7].

Table 1: Reference configuration:

b_{sa}	$0.474[m]$
c_{sa}	$0.097[m]$
l_1	$2.843[m]$
l_2	$.6931[m]$
m	$2942[Kg]$
m_{pn}	$3.65[Kg]$
m_{ce}	$2.75[Kg]$
m_s	$2.719[Kg]$
m_f	$2.015[Kg]$
J_s	$.006932[Kgm^2]$
k_f	1.05226
r_{b1}	$0.031745[m]$
r_{b2}	$0.025375[m]$
r	$.184[m]$
r_{ce}	$.072[m]$
r_{pn}	$.128[m]$
w	$.126[m]$
z	$.08[m]$
p_0	$600000[Pa]$
p_r	$600000[Pa]$
κ	.15
β_z	$0[Ns/rad]$
$\mu_{bearing}$	0.05
x	$0.155124[m]$

Table 2: Reference configuration

l_1	$2.843[m]$
l_2	$.6931[m]$
J_z	$9000[Kgm^2]$
$\beta_{y,2}$	$140[Ns/m]$

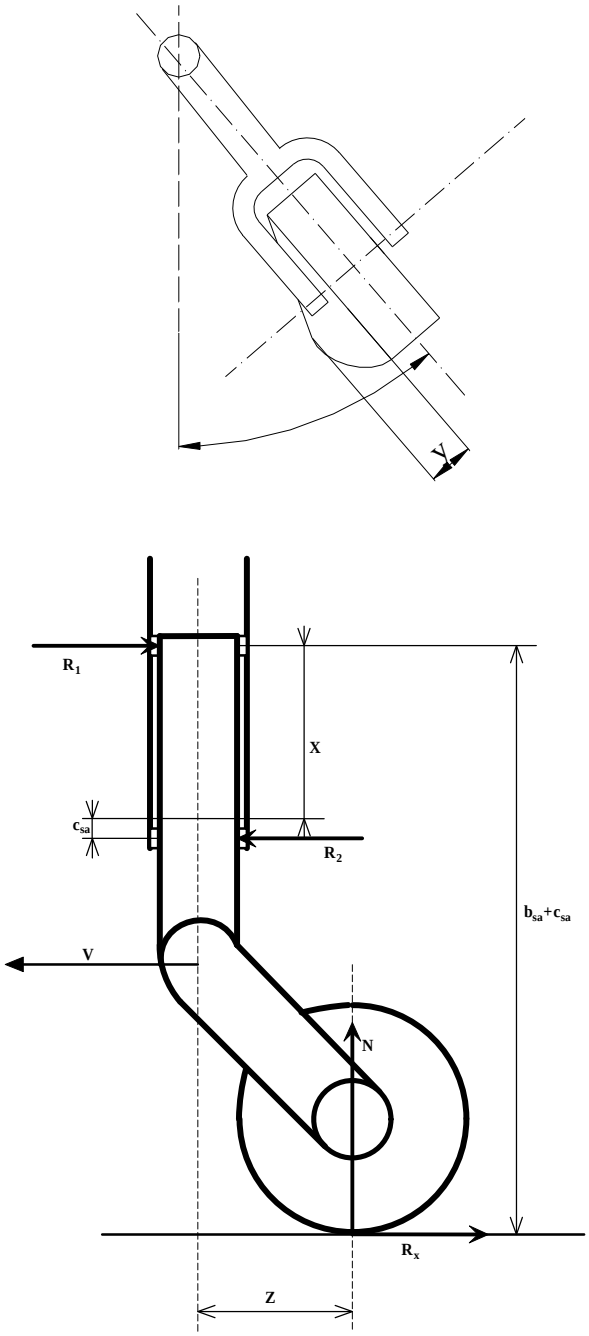

Figure 1: Landing gear

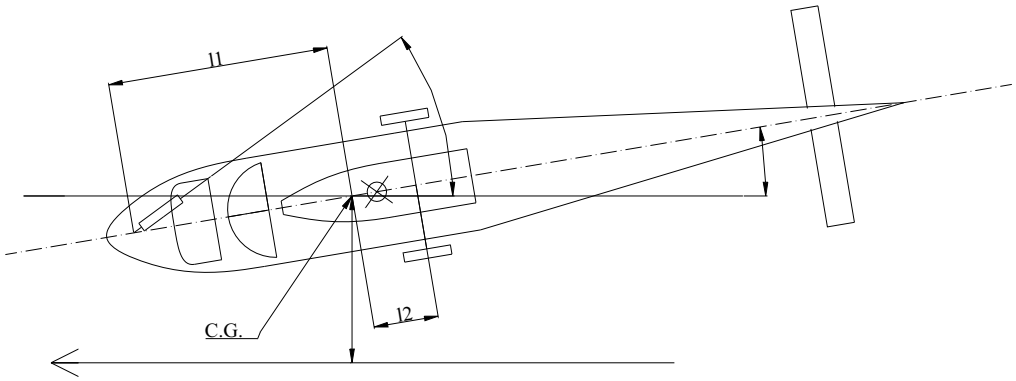

Figure 2: Helicopter.

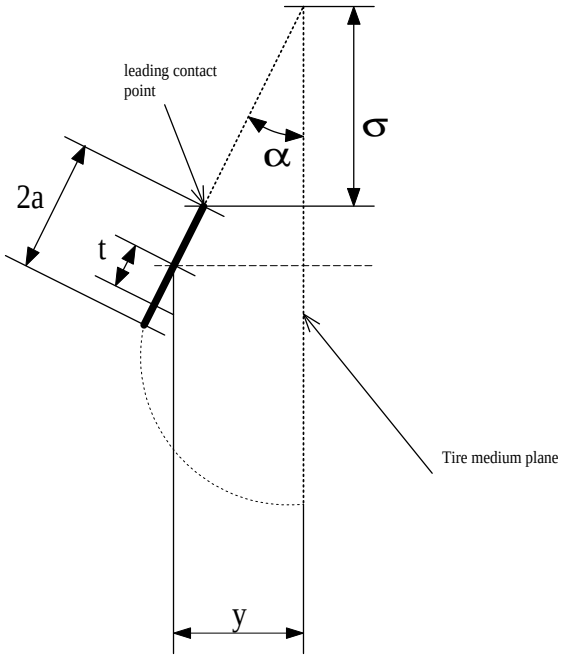

Figure 3: Tire footprint.

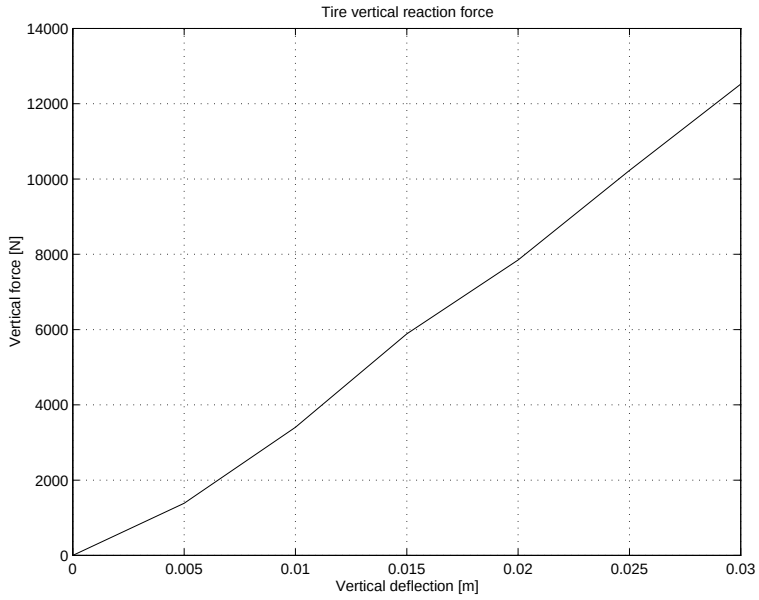

Figure 4: Vertical reaction force vs. vertical deflection (Goodyear 145K21-2")

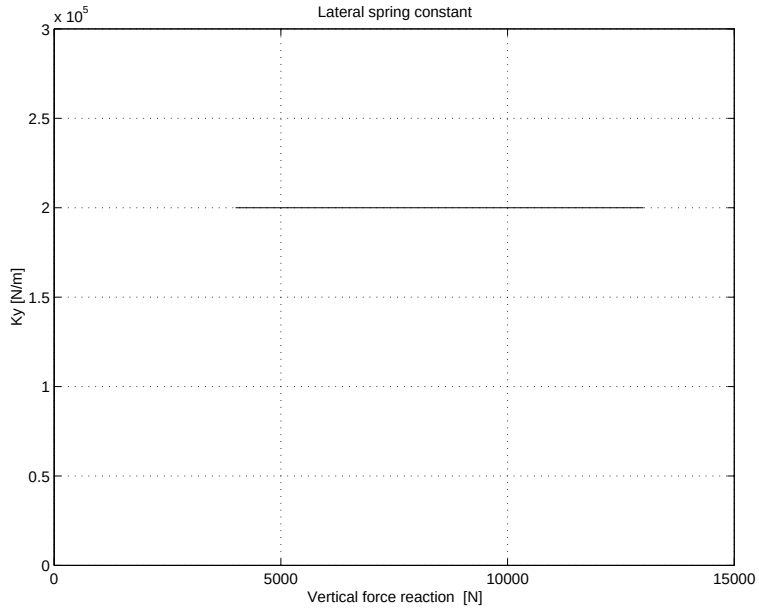

Figure 5: Lateral spring constant vs. vertical reaction force (Goodyear 145K21-2")

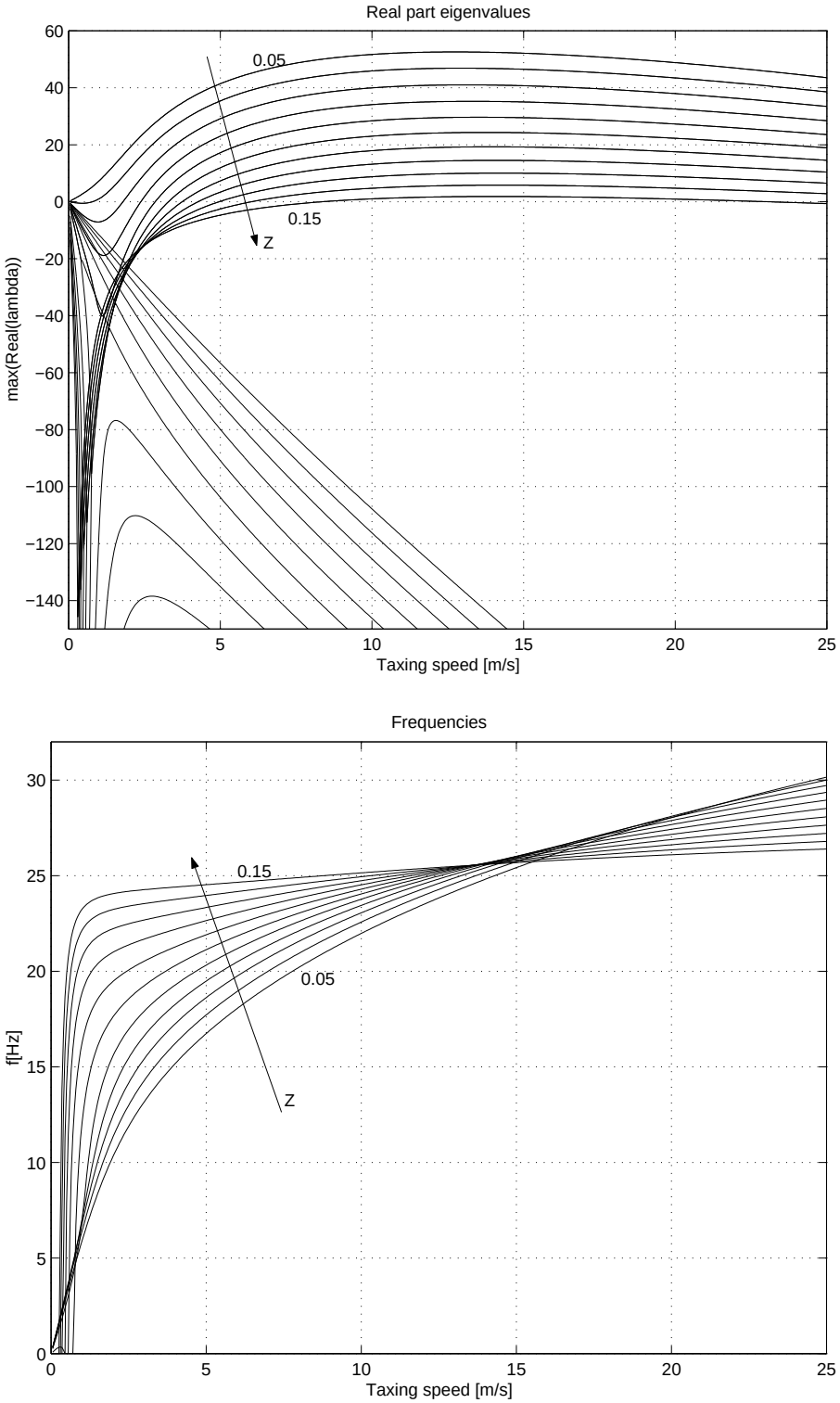

Figure 6: Caster length effect.

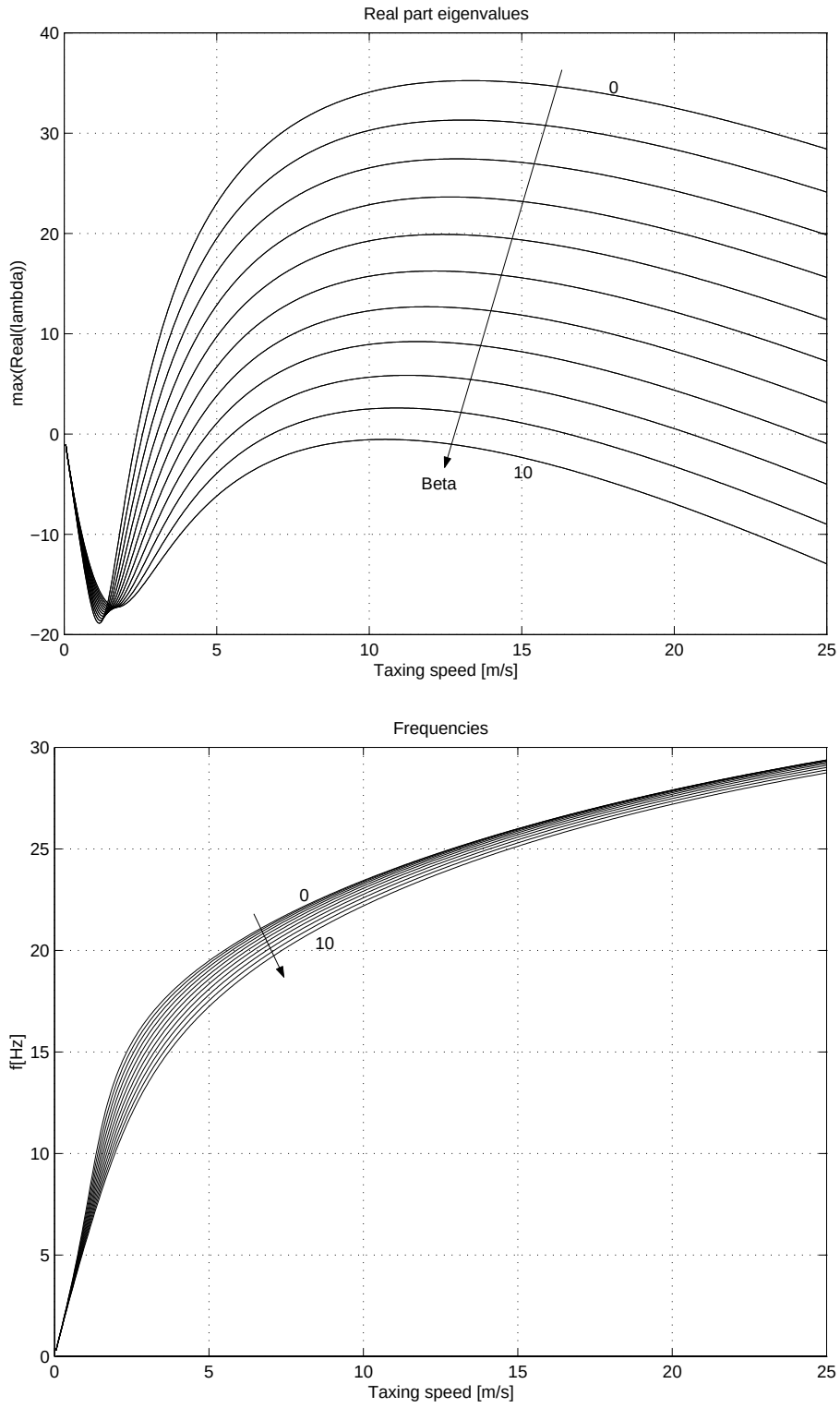

Figure 7: Damping torque effect.

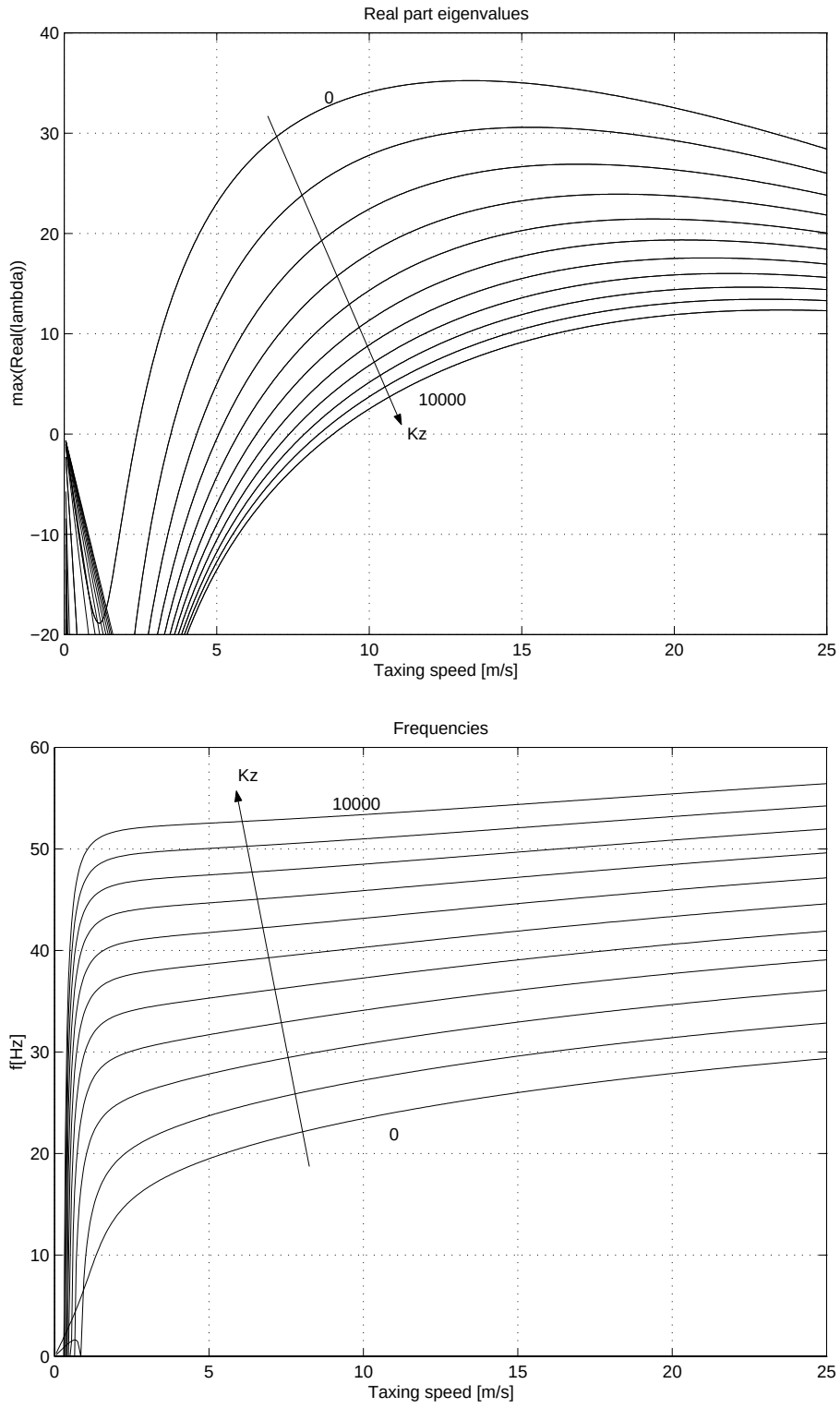

Figure 8: Stem stiffness effect.

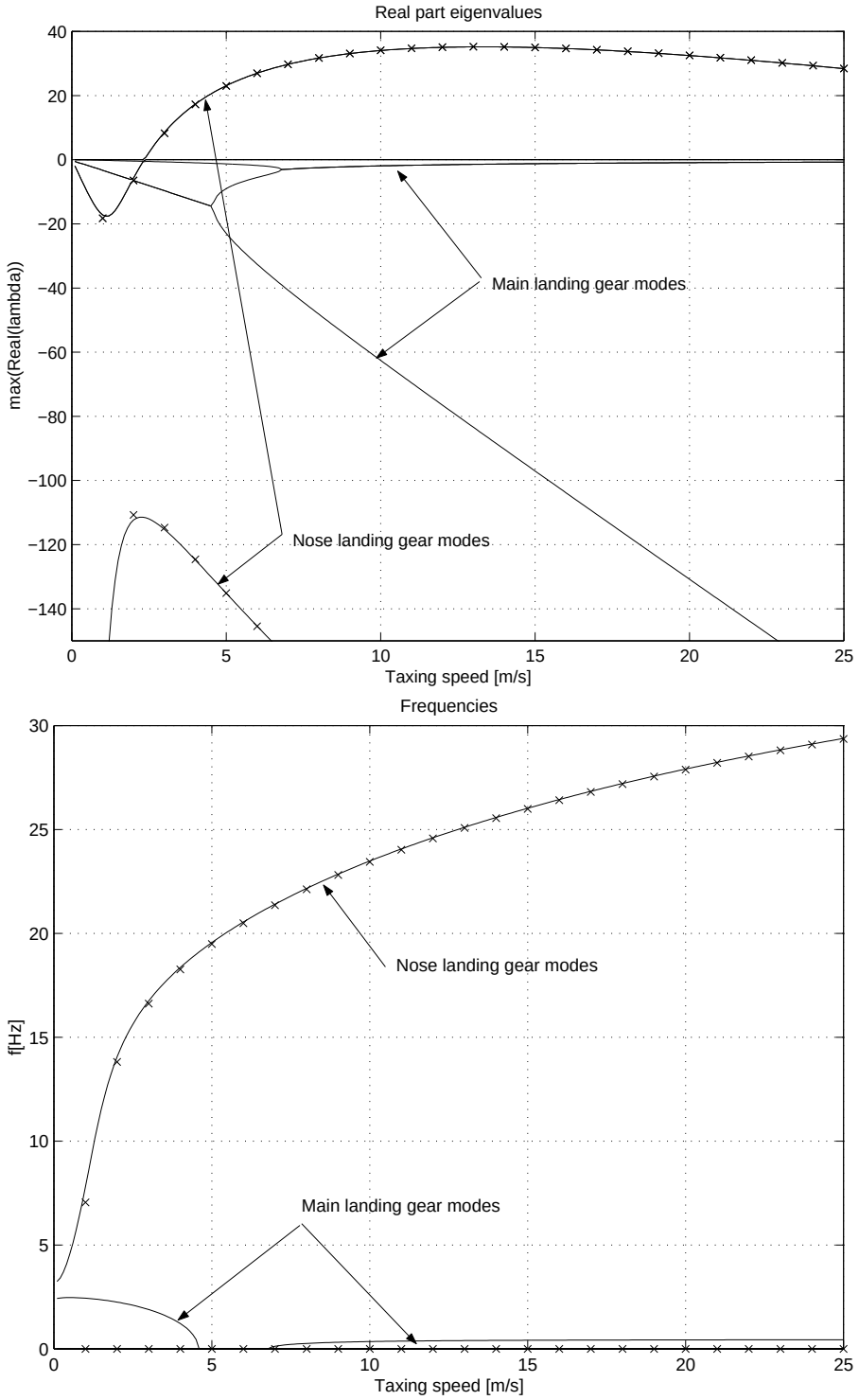

Figure 9: Comparison between 2 dof and 5 dof models.

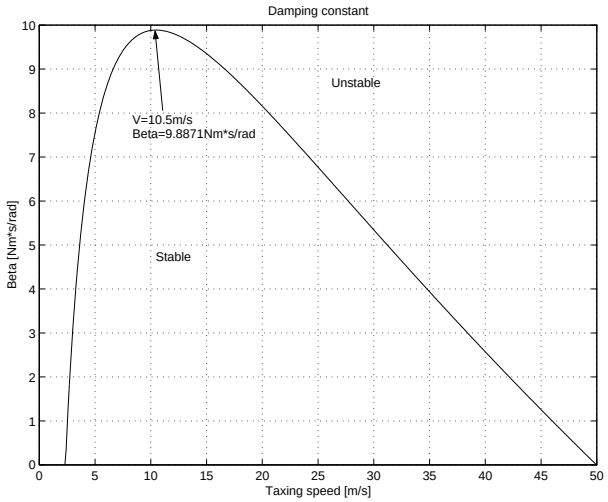

Figure 10: Damping constant.

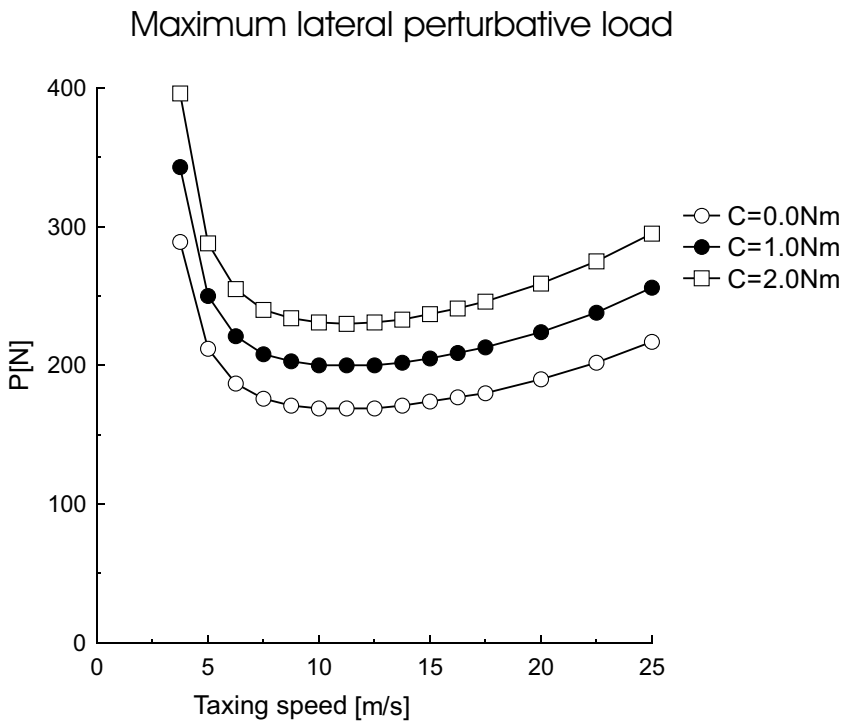

Figure 11: Critical impulsive load

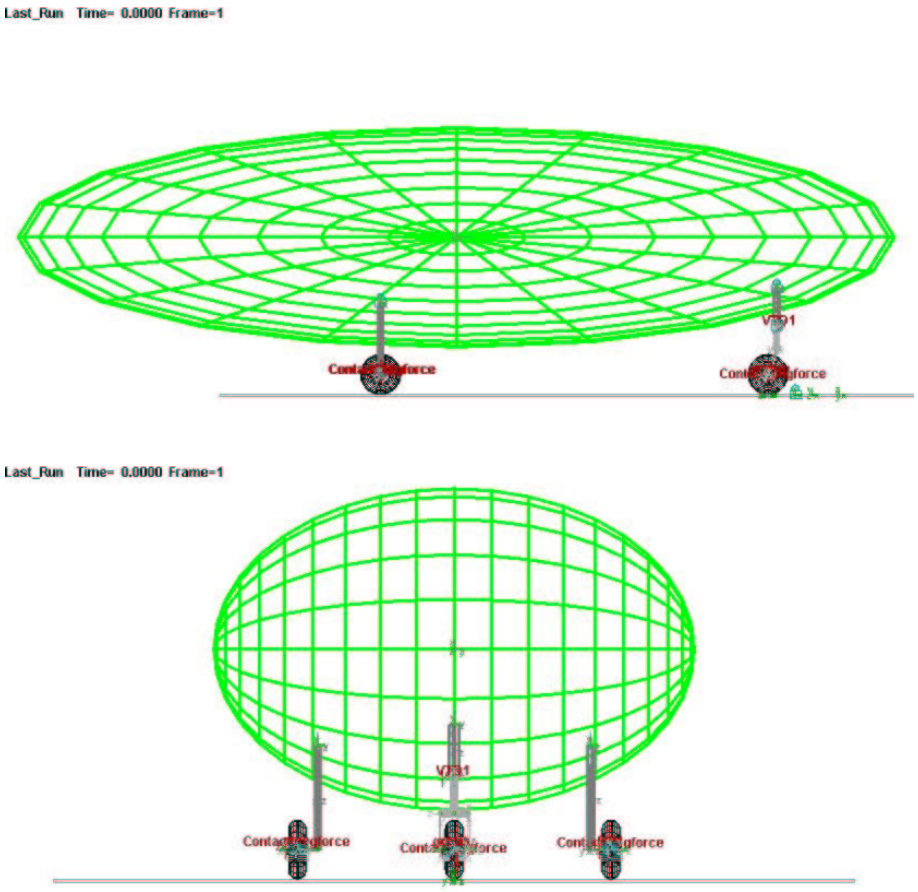

Figure 12: Helicopter views

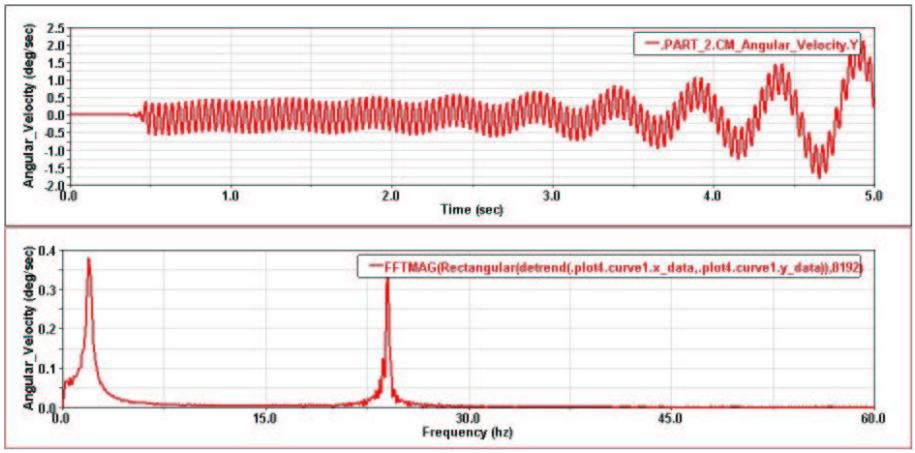

Figure 13: Angular velocity and its FFT-module.

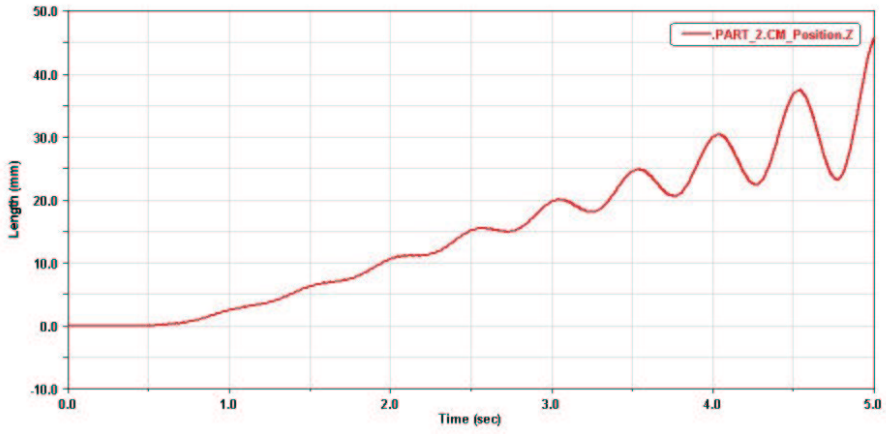

Figure 14: Lateral helicopter shift.

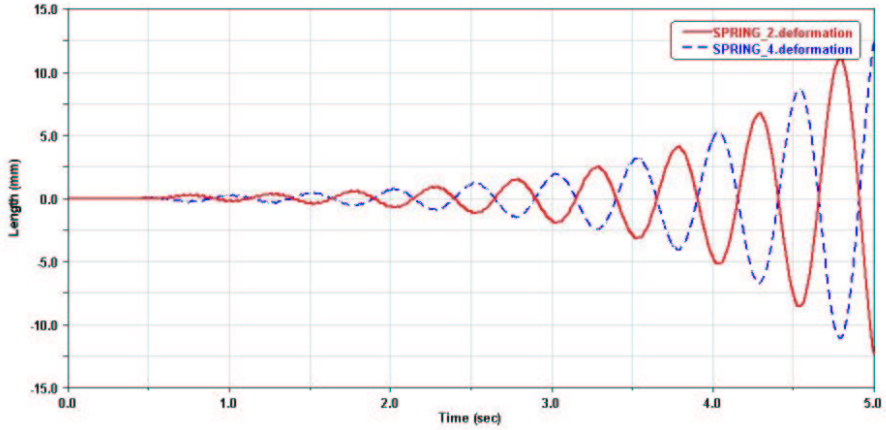

Figure 15: Main landing gear tire lateral distortions.